

# Engineered AXL<sup>-ECD</sup>-Fc variants that abolish the AXL/Gas6 interaction suppress tumor cell migration

YANTING DUAN<sup>1,2</sup>, BO HU<sup>3</sup>, CHUNXIA QIAO<sup>1,2</sup>, LONGLONG LUO<sup>1,2</sup>, XINYING LI<sup>2,4</sup>, JING WANG<sup>1,2</sup>,  
HAO LIU<sup>5</sup>, TINGTING ZHOU<sup>2,4</sup>, BEIFEN SHEN<sup>2,4</sup>, MING LV<sup>2,4</sup> and JIANNAN FENG<sup>1,2</sup>

<sup>1</sup>State Key Laboratory of Toxicology and Medical Countermeasures, Beijing Institute of Pharmacology and Toxicology;

<sup>2</sup>Beijing Key Laboratory of Therapeutic Gene Engineering Antibody, Beijing 100850; <sup>3</sup>Department of

Ultrasound, Union Hospital, Tongji Medical College, Huazhong University of Science and Technology, Wuhan,

Hubei 430022; <sup>4</sup>Laboratory of Immunology, Institute of Military Cognitive and Brain Sciences, Beijing 100850;

<sup>5</sup>Joint National Laboratory for Antibody Drug Engineering, Henan University, Zhengzhou, Henan 475004, P.R. China

Received October 24, 2018; Accepted March 29, 2019

DOI: 10.3892/ol.2019.10255

**Abstract.** AXL receptor tyrosine kinase ligand (AXL), a tyrosine kinase receptor that is commonly overexpressed in numerous types of cancer, significantly promotes drug resistance and metastasis in tumor cells. Inhibition of the AXL/growth arrest-specific 6 (Gas6) signaling pathway is emerging as a potential anticancer therapeutic strategy. In the present study, on the basis of the three-dimensional complex structure of AXL/Gas6, the critical residues (E<sup>56</sup>, E<sup>59</sup> and T<sup>77</sup>) in AXL binding to Gas6 were determined using computer graphics analysis and the distance geometry method. Subsequently, four-variant AXL<sup>-ECD</sup>-Fc-M1 (G<sup>32</sup>S, D<sup>87</sup>G, V<sup>92</sup>A and G<sup>127</sup>R) and AXL<sup>-ECD</sup>-Fc-M2 (G<sup>32</sup>A, D<sup>87</sup>A, V<sup>92</sup>A and G<sup>127</sup>A) were predicted as high-affinity mutants; AXL<sup>-ECD</sup>-Fc-M3 (E<sup>56</sup>R and T<sup>77</sup>R) and AXL<sup>-ECD</sup>-Fc-M4 (E<sup>59</sup>R and T<sup>77</sup>R) were predicted as low-affinity mutants. The results of the present study revealed that the half-maximal effect concentrations of AXL<sup>-ECD</sup>-Fc-M1 and AXL<sup>-ECD</sup>-Fc-M2 were ~0.141 and

0.375  $\mu$ g/ml, respectively, whereas that of the wild-type protein (AXL<sup>-ECD</sup>-Fc-WT) was 0.514  $\mu$ g/ml. Furthermore, adding the high-affinity mutants into culture medium to capture free Gas6 significantly inhibited AXL/Gas6 binding and thus blocked the downstream signaling pathway. In addition, the high-affinity mutants effectively suppressed the migration and metastasis of SKOV3 and A549 cells. Conversely, compared with AXL<sup>-ECD</sup>-Fc-WT, the low-affinity AXL mutants AXL<sup>-ECD</sup>-Fc-M3 and AXL<sup>-ECD</sup>-Fc-M4 lost all inhibitory activities. These findings highlight AXL as a potential therapeutic target and demonstrated that the key residues E<sup>56</sup>, E<sup>59</sup> and T<sup>77</sup> may be crucial sites for abolishing the activity of the AXL/Gas6 pathway in cancer therapy.

## Introduction

Receptor tyrosine kinases (RTKs) are transmembrane proteins whose ligands induce receptor dimerization and activate RTK downstream signaling pathways. RTKs are known to be involved in cell proliferation, survival and differentiation pathways (1,2). As a member of the TYRO3 protein tyrosine kinase, AXL RTK ligand (AXL) and MER RTK (TAM) subfamily of RTKs, AXL has been reported to be a promising oncogenic target owing to its overexpression in several types of human cancer, including various types of leukemia and solid tumors, as well as being an indicator of poor prognosis (3-10). Furthermore, AXL serves a key role in drug resistance (11-17). In addition, growth arrest-specific 6 (Gas6), the major ligand of AXL, has been identified as being expressed in a number of types of human cancer, binding with AXL to activate its phosphorylation and drive AXL/Gas6 signaling. This signaling pathway has been revealed to be associated with the activation of downstream signaling, including mitogen activated protein kinase (MAPK), phosphoinositide 3-kinase (PI3K)/protein kinase B (AKT), and focal adhesion kinase/steroid receptor coactivator/nuclear factor  $\kappa$ -B signaling pathways, to drive tumor cell metastasis, confer therapeutic resistance and promote disease progression (11,18,19).

The crystal structure of a minimal human AXL/Gas6 complex revealed an assembly with 2:2 stoichiometry (20).

*Correspondence to:* Dr Jiannan Feng, State Key Laboratory of Toxicology and Medical Countermeasures, Beijing Institute of Pharmacology and Toxicology, 27 Taiping Road, Beijing 100850, P.R. China

E-mail: fengjiannan1970@qq.com

Dr Ming Lv, Laboratory of Immunology, Institute of Military Cognitive and Brain Sciences, 27 Taiping Road, Beijing 100850, P.R. China

E-mail: lm62033@163.com

*Abbreviations:* TAM, TYRO3 protein tyrosine kinase, AXL receptor tyrosine kinase ligand and MER receptor tyrosine kinase proteins; Gas6, growth arrest-specific 6; RTK, receptor tyrosine kinase; DMEM, Dulbecco's modified Eagle's medium; CVFF, consistent valence force field

*Key words:* AXL receptor tyrosine kinase ligand/growth arrest specific 6 pathway, distance geometry, Fc fusion protein, cell migration, cancer therapy

Further analysis with structure-based mutagenesis, protein binding assays, and receptor activation experiments demonstrated that the major and minor Gas6 binding sites are required for productive transmembrane signaling (20). In a previous study, several AXL antagonists, including antibodies, small molecules and aptamers, were reported to block signaling through the receptor; however, current anti-AXL therapeutics either demonstrate modest antitumor efficacy or induce substantial off-target effects (4,21-25). Kariolis *et al.* (26) examined an AXL-decoy receptor, named MYD1, and revealed that this Fc fusion protein possessed a high affinity to human Gas6. Furthermore, MYD1 could block the native AXL/Gas6 interaction and inhibit cancer cell migration and invasion through the AXL signaling pathway; marked effects were observed in an animal model.

Therefore, the present study aimed to effectively and specifically disrupt the AXL/Gas6 signaling axis according to its three-dimensional (3-D) complex structure. First, the interaction mode of AXL/Gas6 was analyzed using computational biology. Based on the theoretical analysis results, two types of mutations were constructed, and the AXL mutants were added into culture medium to capture free Gas6. The potential effects of these mutations on the AXL/Gas6 signaling pathway were investigated in human cancer cell lines.

## Materials and methods

**Reagents and antibodies.** Recombinant Gas6 human protein (catalog no. 885-GSB) and goat anti-AXL antibodies (catalog no. AF154) (all R&D Systems, Inc., Minneapolis, MN, USA), Rabbit Anti-Goat IgG (H&L) fluorescein isothiocyanate (catalog no. ab6737; Abcam, Cambridge, UK), human full-length pCMV6-AXL plasmid (catalog no. SC112559; OriGene Technologies, Inc., Rockville, MD, USA), TMB Chromogen Solution (catalog no. 183657000; Invitrogen; Thermo Fisher Scientific, Inc., Waltham, MA, USA), RIPA (catalog no. R0010; Beijing Solarbio Science & Technology Co., Ltd., Beijing, China), Giemsa (catalog no. G1010; Beijing Solarbio Science & Technology Co., Ltd.), Taq Blend (catalog no. BTQ-201; Toyobo Life Science, Osaka, Japan) and trypsin-EDTA (0.25%; catalog no. 1967499; Thermo Fisher Scientific, Inc.) were obtained. Lipofectamine<sup>®</sup> 3000 Transfection Reagent (catalog no. L3000001; Invitrogen; Thermo Fisher Scientific, Inc.), fetal bovine serum (FBS; catalog no. 1997802C; Gibco, Gaithersburg, MD, USA), R428 inhibitor (catalog no. HY-15150; ChemCatch, CA, USA), anti-AXL antibodies (catalog no. 4939), anti-phosphorylated (phospho)-AXL (catalog no. 5724), and anti-GADPH antibodies (catalog no. 51332) were obtained from Cell Signaling Technology, Inc. (Danvers, MA, USA), goat anti-human immunoglobulin G (IgG) was from KPL, Inc., (catalog no. 01-10-06; Gaithersburg, MD, USA), and horseradish peroxidase (HRP)-conjugated goat anti-human IgG was from Thermo Fisher Scientific, Inc. (catalog no. A24494). The proteins were purified using the ÄKTAprime<sup>®</sup> plus system (catalog no. 11001313; GE Healthcare, Pittsburgh, PA, USA).

**Cell culture.** SKOV3 (catalog no. HTB-77), A549 (catalog no. CCL-185), H1299 (catalog no. CRL-5803), 293T (catalog no. CRL-3216) and MDA-MB-231

(catalog no. HTB-26) cells (all obtained from American Type Culture Collection, Manassas, VA, USA) were authenticated by Beijing ZhongYuan Company (Beijing, China; <http://www.sinozhongyuan.com>) in 2014. The cells were cultured in Dulbecco's modified Eagle's medium (DMEM; catalog no. 8118210) and McCoy's 5A medium (catalog no. 1835937) supplemented with 10% heat-inactivated FBS (catalog no. 1932594C) (all Gibco; Thermo Fisher Scientific, Inc.) and 100 U/ml penicillin-streptomycin, and cultured in a cell incubator at 37°C with 5% CO<sub>2</sub>.

**Theoretical computational analysis.** All computational and theoretical analyses were performed using InsightII 2000 software (MSI, San Diego, CA) in an IBM Corp. workstation (Armonk, NY, USA). Based on the crystal complex structures of AXL and Gas6 (20), the coordinates of the hydrogen atoms were assigned under a consistent valence force field (CVFF), and the whole complex structure was optimized using the steepest decent and conjugate gradient method (InsightII 2000 software, Discovery mode). With the optimized complex structure, the AXL/Gas6 interaction mode was evaluated using a computer graphics technique and the distance geometry method (InsightII 2000 software, Standard mode). Using Superimposition software (InsightII 2000 software, Standard mode), the complex structure and the orientation of the main-chain carbon atoms were identified, and the comparison of their location was analyzed to determine the 3-D protein structures of AXL and Gas6. Furthermore, using the interaction binding free energy calculation method (InsightII 2000 software, Discovery mode), the binding energy between Gas6 and AXL or its mutants was calculated under the CVFF.

**Construction and transfection.** Using the human full-length pCMV6-AXL plasmid as the template, polymerase chain reaction was performed using Taq Blend kit to obtain AXL<sup>-ECD</sup>-Fc-wild-type (WT) and AXL<sup>-ECD</sup>-Fc-M fragments, AXL<sup>-ECD</sup>-Fc-M1 (G<sup>32</sup>S, D<sup>87</sup>G, V<sup>92</sup>A and G<sup>127</sup>R), AXL<sup>-ECD</sup>-Fc-M2 (G<sup>32</sup>A, D<sup>87</sup>A, V<sup>92</sup>A and G<sup>127</sup>A), AXL<sup>-ECD</sup>-Fc-M3 (E<sup>56</sup>R and T<sup>77</sup>R) and AXL<sup>-ECD</sup>-Fc-M4 (E<sup>59</sup>R and T<sup>77</sup>R) (M1/M2, high-affinity mutations; M3/M4, low-affinity mutations). The thermocycling conditions for AXL<sup>-ECD</sup>-WT were as follows: 94°C for 2 min; 94°C for 30 sec, 62°C for 30 sec, 72°C for 90 sec, 30 cycles; 72°C for 10 min. The target fragments were amplified by p-up (forward)/p1 (reverse), p2 (forward)/p3 (reverse), p4 (forward)/p5 (reverse), p6 (forward)/p-down (reverse) primers (Table I). The PCR conditions were as follows: 94°C for 2 min, 94°C for 30 sec, 62°C for 30 sec and 72°C for 30-90 sec (depending on the fragment length) for 30 cycles; 72°C for 10 min. The recovered four fragments were subjected to overlap PCR to amplify the full-length fragment. Overlap PCR conditions were: No primer reaction: 94°C for 2 min; 94°C for 30 sec, 62°C for 30 sec, 72°C for 90 sec, 7 cycles; 72°C for 10 min. Subsequently, primers were added and a further reaction was performed: 94°C for 30 sec, 62°C for 30 sec, 72°C for 90 sec, 23 cycles; 72°C for 10 min.

The fragments were double-digested using *HindIII* and *NheI*, and ligated to the optimized pCDNA<sup>®</sup>5 plasmid. For the Fc-fusion protein expression, the human Fc gene was subcloned using *HindIII*/*BamHI* enzyme sites to obtain the target protein with Fc fused in the C-terminus). Then, 5 AXL<sup>-ECD</sup>-WT/M

Table I. PCR primer sequences.

Target	Sequence (5'→3')
AXL <sup>-ECD</sup> -WT	p-up: GCCAAGCTTACCACCATGGCGTGGCGGTGCCCCA p-down: GCCCTCGAG TGAAGGTTCTTCACCAGCTGGTGGA
AXL <sup>-ECD</sup> -M1	p-up: GCCAAGCTTACCACCATGGCGTGGCGGTGCCCCA p1: ATTCCCTGGGTTGGACACGAAGGGACTTTC p2: AGTCCCTTCGTGTCCAACCCAGGGAAT p3: GATTCTGAGCTGGCTGGCCACTATCCAGTCTCCCTGTTTCATCCTC p4: GAGGATGAACAGGGGAGACTGGATAGTGGCCAGCCAGCTCAGAATC p5: AGGCAAGCCCTCCAGCCGAACATAGCCAGGCTG p6: CAGCCTGGCTATGTTTCGGCTGGAGGGCTTGCCTTA p-down: GCCCTCGAG TGAAGGTTCTTCACCAGCTGGTGGA
AXL <sup>-ECD</sup> -M2	p-up: GCCAAGCTTACCACCATGGCGTGGCGGTGCCCCA p1: ATATTCCTGGGTTGGCCACGAAGGGACTT p2: AAGTCCCTTCGTGGCCAACCCAGGGAATAT p3: TCTGAGCTGGCTGGCCACTATCCAGTCAGCCTGTTTCATCCTCACC p4: GGTGAGGATGAACAGGCTGACTGGATAGTGGCCAGCCAGCTCAGA p5: CAAGCCCTCCAGCGCAACATAGCCAGGCTGGG p6: CCCAGCCTGGCTATGTTTCGGCTGGAGGGCTTG p-down: GCCCTCGAGTGAAGGTTCTTCACCAGCTGGTGGA
AXL <sup>-ECD</sup> -M3	p-up: GCCAAGCTTACCACCATGGCGTGGCGGTGCCCCA p1: TACCTCGGGGGGCCCTCCCTGAACCTGGAG p2: CTCCAGGTTTCAGGGAGGGCCCCCGAGGTA p3: CCCAGGGGCACCTGGCCCTGGGTGCTGTCC p4: GGACAGCACCCAGGGCCAGGTGCCCTGGG p-down: GCCCTCGAGTGAAGGTTCTTCACCAGCTGGTGGA
AXL <sup>-ECD</sup> -M4	p-up: GCCAAGCTTACCACCATGGCGTGGCGGTGCCCCA p1: AAGCCAATGTACCCGGGGGGGCTCTCC p2: GGAGAGCCCCCGGGTACATTGGCTT p3: CCCAGGGGCACCTGCCGCTGGGTGCTGTCC p4: GACAGCACCCAGCGGCAGGTGCCCTGGG p-down: GCCCTCGAGTGAAGGTTCTTCACCAGCTGGTGGA

AXL, AXL receptor tyrosine kinase ligand; WT, wild type; M, mutant.

fusion proteins were obtained using a Lipofectamine® 3000 transfection system according to the manufacturer's protocol, the 5 recombinant expression vectors were transfected at 20 µg per well into 293T cells (7x10<sup>6</sup> cells/well). At 72 h, the purification of cell culture supernatants was performed using ÄKTA prime plus instrument. SDS-PAGE was used to determine the quality of the purified protein.

**ELISA.** ELISA plates were coated with 0.5 µg/ml Gas6 (100 µl/well) at 4°C overnight. A total of 10 serial 1:3 dilutions of the AXL<sup>-ECD</sup>-Fc-WT/M fusion proteins were obtained (0-15 µg/ml) and added to the plates for 1 h at 37°C. Following three washes, HRP-conjugated goat anti-human IgG (1:2,000) was added as the secondary antibody, and plates were incubated for an additional 30 min at 37°C. Binding signals were visualized using TMB substrate, and the light absorbance was measured using a SPECTRA MAX 190 ELISA reader (Molecular Devices, LLC, Sunnyvale, CA, USA) at 450 nm. Each ELISA experiment was repeated three times.

**Binding kinetics assay.** The binding kinetics of AXL<sup>-ECD</sup>-Fc-WT/M fusion proteins to Gas6 were measured using a BIAcore 3000 instrument (GE Healthcare Bio-Sciences, Pittsburgh, PA, USA). The assays were performed at 30°C in PBS. Sensor tips were pre-wetted for 15 min in the same buffer immediately prior to use, and the microplates were filled with 200 µl/well diluted Gas6 samples or buffer and then agitated at 179 x g. Association (K<sub>on</sub>) and dissociation (K<sub>off</sub>) rates were calculated using a simple 1-to-1 Langmuir binding model (BIAcore Evaluation Software; version 3.2; GE Healthcare Bio-Sciences). The equilibrium dissociation constant (K<sub>d</sub>) was determined using the K<sub>off</sub>/K<sub>on</sub> ratio. The independent measurements were performed three times.

**Flow cytometry.** Flow cytometry was used to detect AXL expression on the cell surface as previously described (27). Briefly, the tumor cells were digested and counted, and 1x10<sup>6</sup> cells per reaction were used. The cells were stained

with goat anti-AXL antibody (catalog no. AF154; 1:500; R&D Systems, Inc.) for 30 min at 4°C, washed three times with buffer, and then incubated with secondary antibodies (1:1,000; rabbit anti-goat IgG FITC; Abcam) for 30 min at 4°C. Once the assay was complete, the cells were washed three times and the expression of AXL was analyzed. To detect the expression of surface AXL, the cell surface FITC intensity was analyzed using a BD FACSCalibur™ flow cytometer (ref. 342975; BD Biosciences, NY, USA) and FlowJo software (version 7.6; BD Biosciences). The flow cytometry experiments were repeated three times.

**Migration assay.** A549 and SKOV3 cells were serum-starved overnight. Following trypsin digestion, the cells were counted and resuspended in serum-free DMEM. Migration assays were performed by seeding  $3 \times 10^4$  cells into BD-Falcon 24 Fluoroblock Transwell inserts with 8- $\mu$ m pores in the upper chamber. For Gas6-dependent migration, 200 ng/ml Gas6 in the presence or absence of 100  $\mu$ g/ml AXL<sup>-ECD</sup>-Fc-WT/M proteins was added to the lower chamber containing the migration medium (DMEM with 5% FBS). R428 (2  $\mu$ M/ml) + Gas6 was used as a control. The AXL<sup>-ECD</sup>-Fc-WT/M protein was added into culture systems to bind free Gas6 and block it from binding with the cell surface AXL protein. Following 4 h of migration, the upper chambers were fixed with 4% paraformaldehyde for 30 min, stained with Giemsa solution for 10 min at room temperature and counted by light microscopy (x10 magnification; Nikon Corporation, Tokyo, Japan) using ImageJ software (version 18.0; National Institutes of Health, MD, USA). The migration experiments were repeated three times.

**Western blot analysis.** Gas6-induced phosphorylation of AXL in SKOV3 cells was detected using western blot analysis. AXL-ECD-Fc WT and its mutant were added to the cell culture as the decoy protein to bind to free Gas6. SKOV3 cells were seeded in 6-well plates ( $5 \times 10^5$  cells/well) for 12 h. The cells were placed in serum-free medium and pre-treated for 8 h with or without AXL-WT/M fusion proteins (10, 2, 0.4 or 0.08  $\mu$ g/ml) at 37°C. Following the addition of 200 ng/ml Gas6 for 30 min in 37°C, cells were collected and lysed in ice-cold RIPA buffer (Beijing Solarbio Science & Technology Co., Ltd.) supplemented with protease inhibitor cocktail (Roche Diagnostics, Basel, Switzerland) for 30 min. Protein concentrations were quantified using a BCA kit (Appligen Technologies, Inc., Beijing, China). Lysates were separated and 20  $\mu$ g protein was loaded per lane using 12% SDS-PAGE, transferred onto a nitrocellulose filter membrane (EMD Millipore, Billerica, MA, USA) and analyzed. Blots were incubated with the primary antibodies anti-AXL, anti-pAXL and anti-GAPDH overnight at 4°C (all antibodies were purchased from Cell Signaling Technology and diluted to 1:1,000). Subsequently, blots were incubated with HRP-conjugated secondary antibodies (1:2,500) for 1 h at room temperature. Immunoreactivity was detected and visualized using an enhanced chemiluminescence detection system (SuperSignal West Pico Trial kit; Pierce; Thermo Fisher Scientific, Inc.) and autoradiography. GAPDH was used as a loading control. Western blot experiments were repeated three times.

**Data analysis.** Statistical analysis was performed using Prism software v.5.0 (GraphPad Software, Inc., La Jolla, CA, USA).

Dunnett's multiple comparisons test was used to compare all other groups to the control group.  $P < 0.05$  was considered to indicate a statistically significant difference. All measurements were within 95% confidence limits.

## Results

**Key amino acid residues in the AXL/Gas6 interaction.** Under CVFF and according to the 3-D crystal complex structure of AXL/Gas6 (20), the coordinates of hydrogen atoms were assigned and optimized using molecular modeling. The theoretical 3-D structures of AXL, Gas6 and the complex structure are presented in Fig. 1A and B. Using the Superimposition software, the main-chain carbon atoms position of the proteins AXL and Gas6 were determined and the orientation of the main-chain carbon atoms was analyzed. The crystal and theoretical structures were then compared. The root mean square deviation value of the main-chain orientation was calculated to be 0.002 nm. The coordinates of the heavy atoms were not altered under assignment of the coordinates of hydrogen atoms; thus, the optimized method and CVFF were suitable in the present study.

On the basis of the theoretical structures of AXL and Gas6, the interaction mode between them was analyzed using a computer graphics technique and the distance geometry method (Fig. 1B). Through investigating the van der Waals interactions and inter-molecular hydrogen bonds, the key amino acid residues through which AXL interacted with Gas6 were determined (Fig. 1C). The influence of the single point mutants of AXL (G<sup>32</sup>, D<sup>87</sup>, V<sup>92</sup>, G<sup>127</sup>, E<sup>56</sup>, E<sup>59</sup> and T<sup>77</sup>) was analyzed; the results revealed that it was not significant and so 4 kinds of mutants were designed. The *in silico* results of the present study revealed that the residues E<sup>56</sup> and E<sup>59</sup> in AXL were bound to Gas6 through electrostatic interactions. In addition, the residue T<sup>77</sup> in AXL was bound to Gas6 through polar interactions. On the basis of the analysis, the 4 mutants, AXL<sup>-ECD</sup>-Fc-M1 (G<sup>32</sup>S, D<sup>87</sup>G, V<sup>92</sup>A and G<sup>127</sup>R), AXL<sup>-ECD</sup>-Fc-M2 (G<sup>32</sup>A, D<sup>87</sup>A, V<sup>92</sup>A and G<sup>127</sup>A), AXL<sup>-ECD</sup>-Fc-M3 (E<sup>56</sup>R and T<sup>77</sup>R) and AXL<sup>-ECD</sup>-Fc-M4 (E<sup>59</sup>R and T<sup>77</sup>R), were designed. In this analysis, the residues E<sup>56</sup> and E<sup>59</sup> in AXL were bound to Gas6 through electrostatic interactions, so E was replaced with R. In addition, the relative binding energy of the 4 mutants to Gas6 compared with the parent AXL was calculated. The results revealed that the relative binding energies of AXL<sup>-ECD</sup>-Fc-M1 and AXL<sup>-ECD</sup>-Fc-M2 were -18.58 and -15.62 kJ/mol, respectively, compared with that of the WT. The relative binding energies of AXL<sup>-ECD</sup>-Fc-M3 and AXL<sup>-ECD</sup>-Fc-M4 were 5.38 and 6.16 kJ/mol, respectively. The results demonstrated that the mutants AXL<sup>-ECD</sup>-Fc-M1 and AXL<sup>-ECD</sup>-Fc-M2 possessed stronger binding affinity to Gas6 than the parent AXL; whereas the mutants AXL<sup>-ECD</sup>-Fc-M3 and AXL<sup>-ECD</sup>-Fc-M4 exhibited lower affinity.

**AXL<sup>-ECD</sup>Fc fusion variants bind with Gas6.** 293T cells did not express the AXL protein (Fig. 2A). The plasmids of AXL<sup>-ECD</sup>-Fc WT and mutants transfected into the 293T cells resulted in an increase in AXL Fc WT and mutant expression, respectively (Fig. 2A). The 5 recombinant expression vectors were transfected into the 293T cells and the proteins were

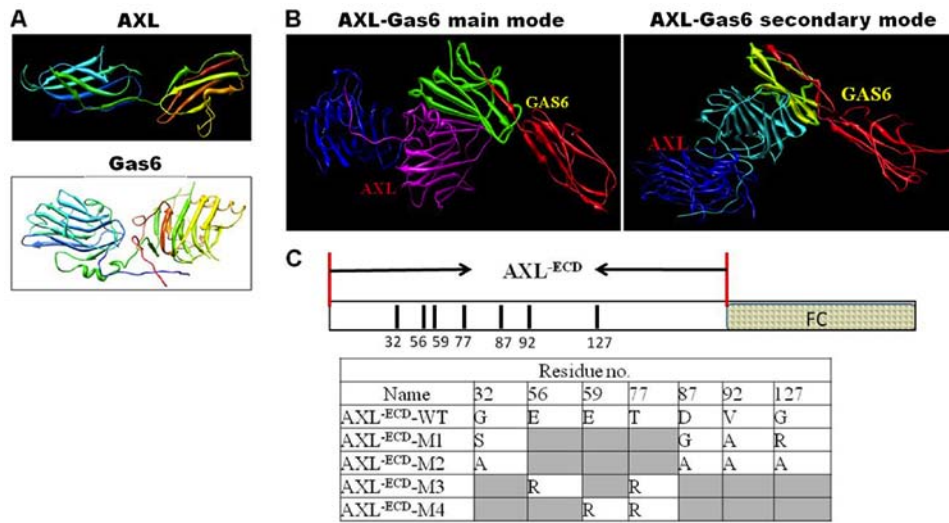


Figure 1. Key amino acid residues of AXL affect its interaction with Gas6. Using structural superimposition, the crystal and theoretical structures of AXL and Gas6 were compared, and the AXL/Gas6 interaction containing primary and secondary modes was determined. The whole complex structure was optimized using the steepest descent and conjugate gradient method. (A) 3-D structure of AXL and Gas6. (B) 3-D structure presenting the interaction mode of the AXL/Gas6 extracellular domain. (C) Key sites were selected, and AXL<sup>ECD</sup>-Fc mutations were generated. AXL<sup>ECD</sup>-Fc-M1 (G32S, D87G, V92A and G127R) and AXL<sup>ECD</sup>-Fc-M2 (G32A, D87A, V92A and G127A) are high-affinity mutations; AXL<sup>ECD</sup>-Fc-M3 (E56R and T77R) and AXL<sup>ECD</sup>-Fc-M4 (E59R and T77R) are low-affinity mutations. AXL, AXL receptor tyrosine kinase ligand; Gas6, growth arrest-specific 6.

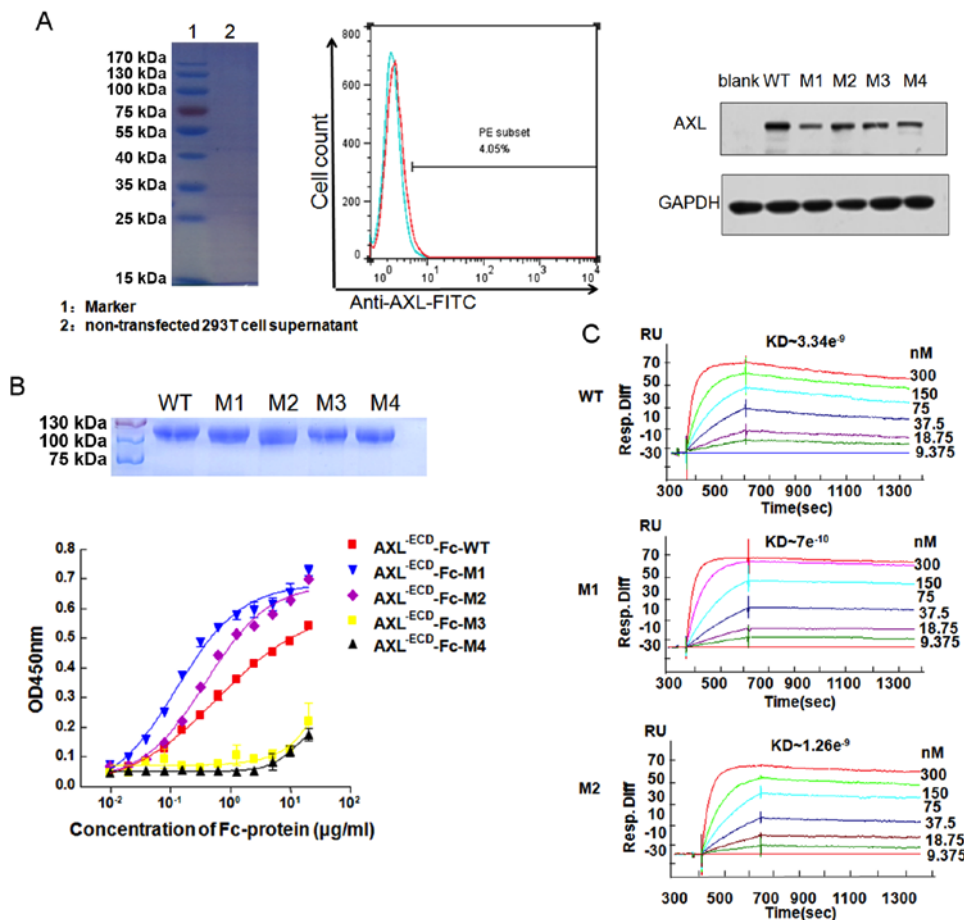


Figure 2. Binding of AXL<sup>ECD</sup>-Fc-WT/M fusion proteins with Gas6. (A) The SDS-PAGE results (left panel) revealed that the untransfected 293T cell culture supernatants did not express AXL protein. The results of the flow cytometry analysis (middle panel) revealed that no AXL was expressed on the 293T cell surface. The western blot analysis (right panel) revealed that the 5 transfected AXL<sup>ECD</sup>-Fc fusion proteins were expressed in the 293T cells. (B) The 5 AXL<sup>ECD</sup>-Fc fusion proteins were obtained using a Lipofectamine<sup>®</sup> 3000 transfection system to transfect the five recombinant expression vectors into 293T cells, followed by purification of cell supernatants after 48 h. SDS-PAGE detected the molecular weights of AXL<sup>ECD</sup>-Fc-WT/M proteins, as presented in the top panel. The bottom panel represents the ELISA analysis of the interaction between the 5 AXL<sup>ECD</sup>-Fc-WT/M fusion proteins and Gas6. (C) BIAcore analysis of the affinities between the 5 AXL<sup>ECD</sup>-Fc-WT/M fusion proteins and Gas6. AXL, AXL receptor tyrosine kinase ligand; Gas6, growth arrest-specific 6; WT, wild-type; RU, Reaction values; Resp. diff, Different reaction values; OD, optical density.

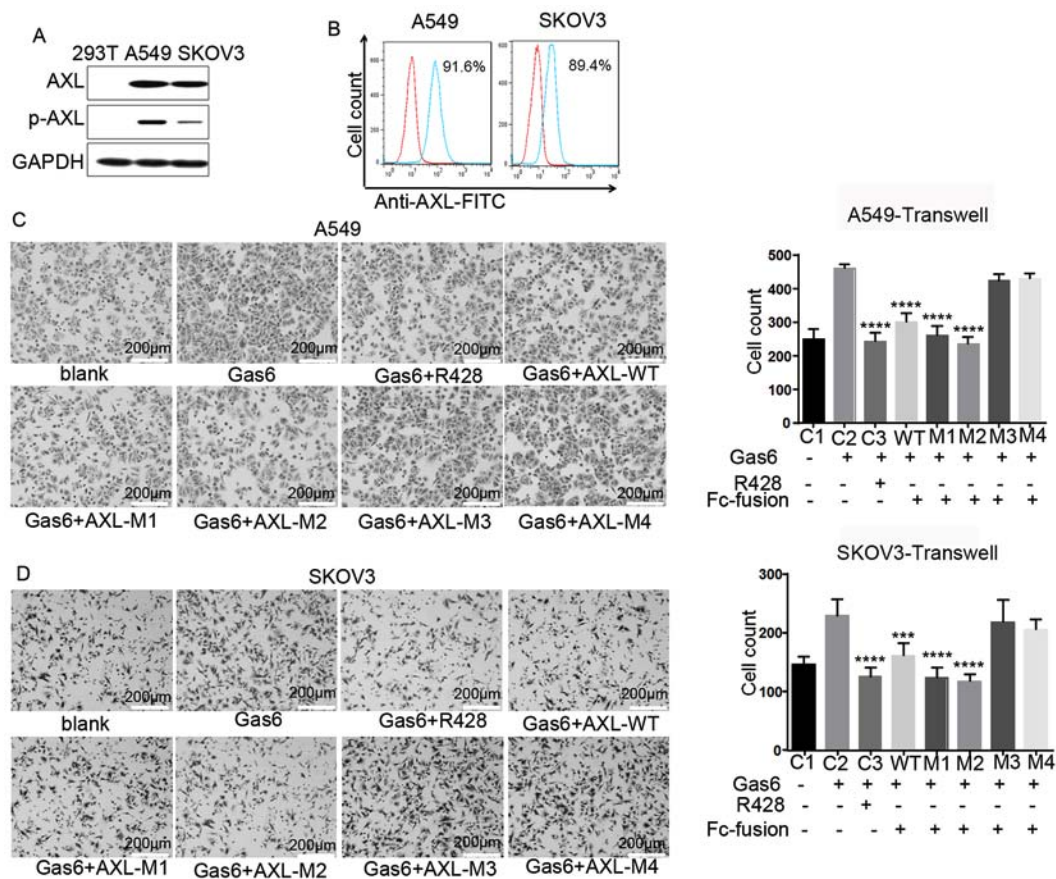


Figure 3. AXL<sup>ECD</sup>-Fc-WT/M fusion proteins inhibited migration in SKOV3 and A549 cells. (A) Total AXL expression in cancer cell lines A549 (carcinoma), SKOV3 (human ovarian cancer cell) and 293T cells. (B) Flow cytometry analysis of the expression of AXL on the SKOV3 and A549 cell surface. Transwell assay results for high-affinity AXL<sup>ECD</sup>-Fc-M1/M2 fusion proteins or low-affinity AXL<sup>ECD</sup>-Fc-M3/M4 fusion proteins, which were added into cell culture medium, to capture free Gas6 in (C) A549 and (D) SKOV3 cells. \*\*\**P*<0.005 and \*\*\*\**P*<0.0001 vs. Gas6 (C2 group). AXL, AXL receptor tyrosine kinase ligand; Gas6, growth arrest-specific 6.

purified from the supernatants. Molecular weight of purified recombinants were verified using SDS-PAGE (Fig. 2B). The ELISA demonstrated that AXL<sup>ECD</sup>-Fc-WT, AXL<sup>ECD</sup>-Fc-M1 and AXL<sup>ECD</sup>-Fc-M2 could bind to Gas6 in a concentration-dependent manner (Fig. 2B). In addition, the half maximal effective concentration values of AXL<sup>ECD</sup>-Fc-M1 and AXL<sup>ECD</sup>-Fc-M2 were 0.141 and 0.375  $\mu\text{g/ml}$ , respectively, whereas that of AXL<sup>ECD</sup>-Fc-WT was 0.514  $\mu\text{g/ml}$ , indicating that AXL<sup>ECD</sup>-Fc-M1 and AXL<sup>ECD</sup>-Fc-M2 possessed stronger binding affinity than AXL<sup>ECD</sup>-Fc-WT. In contrast, AXL<sup>ECD</sup>-Fc-M3 and AXL<sup>ECD</sup>-Fc-M4 had low binding affinity for Gas6. Additional BIAcore experiments (Fig. 2C) yielded the same results.

The  $K_d$  was determined using the  $K_{off}/K_{on}$  ratio. As AXL<sup>ECD</sup>-Fc-M3 and AXL<sup>ECD</sup>-Fc-M4 were low-affinity variants, they exhibited markedly low binding to Gas6 (Fig. S1). In contrast, the  $K_d$  values of AXL<sup>ECD</sup>-Fc-M1 and AXL<sup>ECD</sup>-Fc-M2 were  $7 \times 10^{-10}$  and  $1.48 \times 10^{-9}$  M, respectively, indicating higher affinity compared with that of AXL<sup>ECD</sup>-Fc-WT ( $K_d$ ,  $3.34 \times 10^{-9}$  M).

**AXL<sup>ECD</sup>-Fc fusion variants inhibit cell migration.** The western blot analysis revealed that AXL was expressed in A549 and SKOV3 cells, but not in 293T cells (Fig. 3A), and the flow cytometry results revealed that it was expressed

on the cell surface (Fig. 3B). Expression of AXL was also observed in other cell lines, such as H1299 and MDA-MB-231; however, these cells had a strong autophosphorylation level of AXL, so GAS6 was unable to trigger the phosphorylation of AXL, thus the two cell lines was unsuitable as cell models in the current study (Fig. S2). Therefore, A549 and SKOV3 cells were selected for subsequent experimentation. To investigate the potential function of AXL<sup>ECD</sup>-Fc-WT/M fusion proteins, a Transwell assay was performed. The purified Fc fusion protein was added into culture systems to bind free Gas6 and prevent it from binding to the cell surface AXL protein. The results revealed that AXL<sup>ECD</sup>-Fc-WT, AXL<sup>ECD</sup>-Fc-M1 and AXL<sup>ECD</sup>-Fc-M2 inhibited the migration of A549 and SKOV3 cells induced by free Gas6 compared with that observed with Gas6 alone, consistent with results obtained with the AXL inhibitor R428 (Fig. 3C and D). In contrast, neither AXL<sup>ECD</sup>-Fc-M3 nor AXL<sup>ECD</sup>-Fc-M4 inhibited cell migration promoted by free Gas6. In summary, AXL<sup>ECD</sup>-Fc-WT/M1/M2 fusion proteins inhibited free Gas6-induced cell migration, whereas the AXL<sup>ECD</sup>-Fc-M3/M4 variants demonstrated no such inhibitory function.

**AXL<sup>ECD</sup>-Fc fusion variants block AXL phosphorylation in SKOV3 cells.** Gas6 binds to the extracellular domain of AXL

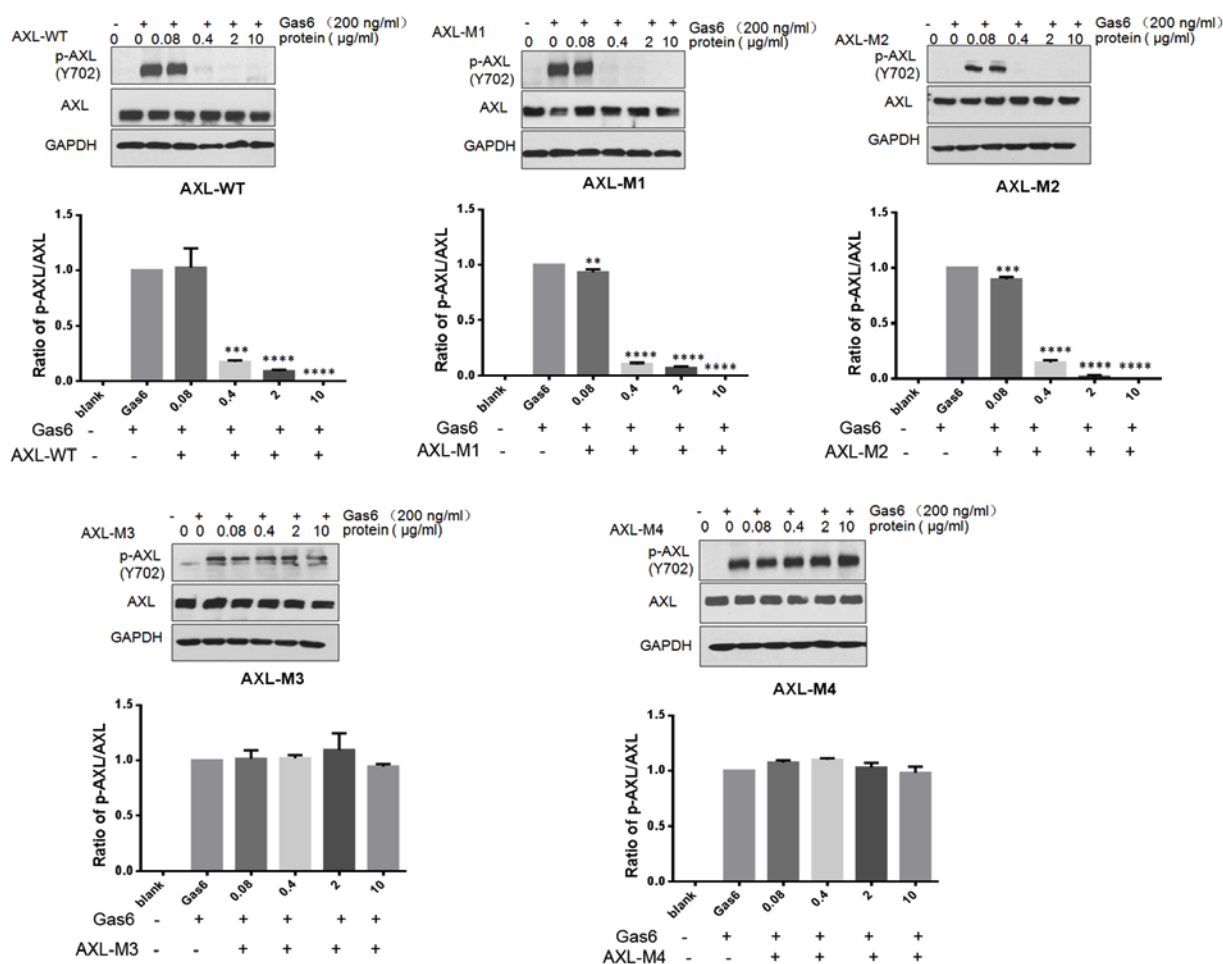


Figure 4. AXL<sup>ECD</sup>-Fc-WT/M fusion proteins alter p-AXL levels in cancer cells. Western blot analysis of changes in p-AXL levels in cells blocked by AXL<sup>ECD</sup>-Fc-M fusion proteins. The numbers below the 'p-AXL' column denote the grey density ratio of p-AXL/GAPDH. \*\*P<0.01, \*\*\*P<0.001 and \*\*\*\*P<0.0001 vs. Gas6. AXL, AXL receptor tyrosine kinase ligand; Gas6, growth arrest-specific 6; p, phosphorylated.

to induce autophosphorylation of tyrosine residues on the intracellular tyrosine kinase domain of AXL, subsequently activating the MAPK/extracellular signal-regulated kinase and PI3K/AKT signaling pathways. This results in the modulation of numerous cellular activities, including cell survival, proliferation, migration, invasion and drug resistance (17,28,29). Therefore, the effects of AXL<sup>ECD</sup>-Fc-WT/M fusion proteins on Gas6-induced AXL signaling pathways were investigated in SKOV3 cells through analyzing AXL phosphorylation by western blotting (Fig. 4). Briefly, cells were pretreated with the indicated concentrations of AXL<sup>ECD</sup>-Fc-WT/M fusion proteins for 8 h prior to stimulation with Gas6. The results revealed that free Gas6 treatment induced AXL phosphorylation, whereas AXL<sup>ECD</sup>-Fc-WT/M1/M2 fusion protein pretreatment resulted in a concentration-dependent decrease in phosphorylation. Furthermore, the overall level of AXL expression was not changed by AXL<sup>ECD</sup>-Fc-WT/M fusion protein treatment. These results suggest that AXL<sup>ECD</sup>-Fc-WT/M1/M2 fusion proteins neutralize the free Gas6 protein, preventing the interaction between Gas6 and AXL in SKOV3 cells. This leads to the obstruction of the Gas6-induced phosphorylation of AXL, and the downregulation of the AXL/Gas6 downstream signaling pathway.

## Discussion

In the present study, the key amino acid residues in AXL that affect its interaction with Gas6 were identified (E<sup>56</sup>, E<sup>59</sup> and T<sup>77</sup>). Furthermore, the inhibition of the AXL/Gas6 signaling pathway using high-affinity mutants resulted in the inhibition of cancer cell migration. AXL<sup>ECD</sup>-Fc-M1 and -M2, which were identified as high-affinity mutations, blocked the functions of AXL/Gas6 by decreasing AXL phosphorylation. Cancer cell migration induced by Gas6 was also inhibited. AXL<sup>ECD</sup>-Fc-M3 and AXL<sup>ECD</sup>-Fc-M4 were characterized as low-affinity mutations, supporting the notion that the amino acid T<sup>77</sup> serves a key role in AXL binding to Gas6.

RTK activation is believed to result from ligand-induced receptor dimerization, leading to the autophosphorylation of multiple tyrosine residues in the cytosolic domains and affecting downstream signaling (30). In cancer, the AXL signaling pathway can be activated by Gas6 in an autocrine or paracrine manner (5-8). The functional role of AXL/Gas6 signaling within the tumor microenvironment has previously been reported to promote tumor progression, and nutrient deprivation within the tumor microenvironment may contribute to activation of the AXL/Gas6 signaling pathway (31). In addition, AXL has been identified as a direct

transcriptional target of hypoxia-inducible factor (HIF)-1 and HIF-2 in tumor cells (31). In several studies, anti-AXL antibodies were reported to block the AXL/Gas6 interaction and inhibit AXL downstream signaling; however, tumor migration and invasion were not altered, and tumor progression was not effectively inhibited (25,32). Thus, although the roles of the AXL signaling pathway in tumor migration, invasion and inflammation have been extensively studied, the mechanisms mediating these inhibitory effects have not yet been elucidated.

In the present study, the high-affinity mutants AXL<sup>ECD</sup>-Fc-M1 and AXL<sup>ECD</sup>-Fc-M2 demonstrated higher Gas6 binding ability than AXL<sup>ECD</sup>-Fc-WT, resulting in the inhibition of Gas6-induced cancer cell migration. The low-affinity mutants AXL<sup>ECD</sup>-Fc-M3 and AXL<sup>ECD</sup>-Fc-M4 could not block the AXL/Gas6 interaction by binding with Gas6, and the inhibitory function was abolished, indicating that the mutation sites of AXL<sup>ECD</sup>-Fc-M3/M4 served key roles in the AXL/Gas6 interaction. Overall, the results of the present study support that mutation of the amino acid T<sup>77</sup> in AXL inhibits the interaction between AXL and Gas6. Further studies are required to determine the details of the interactions between AXL and Gas6 using small molecule tyrosine kinase inhibitors or antibodies. The present findings may provide an important reference for designing such inhibitors or antibodies, as well as critical insights into future preclinical and clinical studies of AXL in cancer.

#### Acknowledgements

Not applicable.

#### Funding

The National Natural Science Foundation of China provided funding for the present study (grant no. 31771010).

#### Availability of data and materials

The datasets used and/or analyzed during the present study are available from the corresponding author upon reasonable request.

#### Authors' contributions

BS, ML and JF designed the study. YD, JW, HL and XL performed the experiments. YD conducted the primary research. BH, CQ, LL and TZ analyzed the data. YD wrote the manuscript.

#### Ethics approval and consent to participate

Not applicable.

#### Patient consent for publication

Not applicable.

#### Competing interests

The authors declare that they have no competing interests.

#### References

- Lemmon MA and Schlessinger J: Cell signaling by receptor tyrosine kinases. *Cell* 141: 1117-1134, 2010.
- Myers SH, Brunton VG and Unciti-Broceta A: AXL inhibitors in cancer: A medicinal chemistry perspective. *J Med Chem* 59: 3593-3608, 2016.
- Graham DK, DeRyckere D, Davies KD and Earp HS: The TAM family: Phosphatidyserine sensing receptor tyrosine kinases gone awry in cancer. *Nat Rev Cancer* 14: 769-785, 2014.
- Holland SJ, Pan A, Franci C, Hu Y, Chang B, Li W, Duan M, Torneros A, Yu J, Heckrodt TJ, *et al*: R428, a selective small molecule inhibitor of Axl kinase, blocks tumor spread and prolongs survival in models of metastatic breast cancer. *Cancer Res* 70: 1544-1554, 2010.
- Paccez JD, Vogelsang M, Parker MI and Zerbini LF: The receptor tyrosine kinase Axl in cancer: Biological functions and therapeutic implications. *Int J Cancer* 134: 1024-1033, 2014.
- Sheridan C: First Axl inhibitor enters clinical trials. *Nat Biotechnol* 31: 775-776, 2013.
- Gjerdrum C, Tiron C, Høiby T, Stefansson I, Haugen H, Sandal T, Collett K, Li S, McCormack E, Gjertsen BT, *et al*: Axl is an essential epithelial-to-mesenchymal transition-induced regulator of breast cancer metastasis and patient survival. *Proc Natl Acad Sci USA* 107: 1124-1129, 2010.
- Koorstra JB, Karikari CA, Feldmann G, Bisht S, Rojas PL, Offerhaus GJ, Alvarez H and Maitra A: The Axl receptor tyrosine kinase confers an adverse prognostic influence in pancreatic cancer and represents a new therapeutic target. *Cancer Biol Ther* 8: 618-626, 2009.
- Wu CW, Li AF, Chi CW, Lai CH, Huang CL, Lo SS, Lui WY and Lin WC: Clinical significance of AXL kinase family in gastric cancer. *Anticancer Res* 22: 1071-1080, 2012.
- Sainaghi PP, Castello L, Bergamasco L, Galletti M, Bellosti P and Avanzi GC: Gas6 induces proliferation in prostate carcinoma cell lines expressing the Axl receptor. *J Cell Physiol* 204: 36-44, 2005.
- Konieczkowski DJ, Johannessen CM, Abudayyeh O, Kim JW, Cooper ZA, Piris A, Frederick DT, Barzily-Rokni M, Straussman R, Haq R, *et al*: A melanoma cell state distinction influences sensitivity to MAPK pathway inhibitors. *Cancer Discov* 4: 816-827, 2014.
- Hong J, Peng D, Chen Z, Sehdev V and Belkhiri A: ABL regulation by AXL promotes cisplatin resistance in esophageal cancer. *Cancer Res* 73: 331-340, 2013.
- Hong CC, Lay JD, Huang JS, Cheng AL, Tang JL, Lin MT, Lai GM and Chuang SE: Receptor tyrosine kinase AXL is induced by chemotherapy drugs and overexpression of AXL confers drug resistance in acute myeloid leukemia. *Cancer Lett* 268: 314-324, 2008.
- Zhang Z, Lee JC, Lin L, Olivas V, Au V, LaFramboise T, Abdel-Rahman M, Wang X, Levine AD, Rho JK, *et al*: Activation of the AXL kinase causes resistance to EGFR-targeted therapy in lung cancer. *Nat Genet* 44: 852-860, 2012.
- Müller J, Krijgsman O, Tsoi J, Robert L, Hugo W, Song C, Kong X, Possik PA, Cornelissen-Steijger PD, Geukes Foppen MH, *et al*: Low MITF/AXL ratio predicts early resistance to multiple targeted drugs in melanoma. *Nat Commun* 5: 5712, 2014.
- Zhou L, Liu XD, Sun M, Zhang X, German P, Bai S, Ding Z, Tannir N, Wood CG, Matin SF, *et al*: Targeting MET and AXL overcomes resistance to sunitinib therapy in renal cell carcinoma. *Oncogene* 35: 2687-2697, 2016.
- Miller MA, Oudin MJ, Sullivan RJ, Wang SJ, Meyer AS, Im H, Frederick DT, Tadros J, Griffith LG, Lee H, *et al*: Reduced proteolytic shedding of receptor tyrosine kinases is a post-translational mechanism of kinase inhibitor resistance. *Cancer Discov* 6: 382-399, 2016.
- Nagata K, Nakano T, Arita H, Zong C, Hanafusa H and Mizuno K: Identification of the product of growth arrest-specific gene 6 as a common ligand for Axl, Sky, and Mer receptor tyrosine kinases. *J Biol Chem* 271: 30022-30027, 1996.
- Varnum BC, Young C, Elliott G, Garcia A, Bartley TD, Fridell YW, Hunt RW, Trail G, Clogston C, Toso RJ, *et al*: Axl receptor tyrosine kinase stimulated by the vitamin K-dependent protein encoded by growth-arrest-specific gene 6. *Nature* 373: 623-626, 1995.
- Sasaki T, Knyazev PG, Clout NJ, Cheburkin Y, Göhring W, Ullrich A, Timpl R and Hohenester E: Structural basis for Gas6-Axl signalling. *EMBO J* 25: 80-87, 2006.

21. Yan SB, Peek VL, Ajamie R, Buchanan SG, Graff JR, Heidler SA, Hui YH, Huss KL, Konicek BW, Manro JR, *et al*: LY2801653 is an orally bioavailable multi-kinase inhibitor with potent activity against MET, MST1R, and other oncoproteins, and displays anti-tumor activities in mouse xenograft models. *Invest New Drugs* 31: 833-844, 2013.
22. Leconet W, Larbouret C, Chardès T, Thomas G, Neiveyans M, Busson M, Jarlier M, Radosevic-Robin N, Pugnère M, Bernex F, *et al*: Preclinical validation of AXL receptor as a target for antibody-based pancreatic cancer immunotherapy. *Oncogene* 33: 5405-5414, 2014.
23. Cerchia L, Esposito CL, Camorani S, Rienzo A, Stasio L, Insabato L, Affuso A and de Franciscis V: Targeting Axl with a high-affinity inhibitory aptamer. *Mol Ther* 20: 2291-2303, 2012.
24. Paolino M, Choidas A, Wallner S, Pranjic B, Uribealago I, Loeser S, Jamieson AM, Langdon WY, Ikeda F, Fededa JP, *et al*: The E3 ligase Cbl-b and TAM receptors regulate cancer metastasis via natural killer cells. *Nature* 507: 508-512, 2014.
25. Ye X, Li Y, Stawicki S, Couto S, Eastham-Anderson J, Kallop D, Weimer R, Wu Y and Pei L: An anti-Axl monoclonal antibody attenuates xenograft tumor growth and enhances the effect of multiple anticancer therapies. *Oncogene* 29: 5254-5264, 2010.
26. Kariolis MS, Miao YR, Jones DS II, Kapur S, Mathews II, Giaccia AJ and Cochran JR: An engineered Axl 'decoy receptor' effectively silences the Gas6-Axl signaling axis. *Nat Chem Biol* 10: 977-983, 2014.
27. Boshuizen J, Koopman LA, Krijgsman O, Shahrabi A, van den Heuvel EG, Ligtenberg MA, Vredevoogd DW, Kemper K, Kuilman T, Song JY, *et al*: Cooperative targeting of melanoma heterogeneity with an AXL antibody-drug conjugate and BRAF/MEK inhibitors. *Nat Med* 24: 203-212, 2018.
28. Chen PX, Li QY and Yang Z: Axl and prostaticin are biomarkers for prognosis of ovarian adenocarcinoma. *Ann Diagn Pathol* 17: 425-429, 2013.
29. Darling RJ and Brault PA: Kinetic exclusion assay technology: Characterization of molecular interactions. *Assay Drug Dev Technol* 2: 647-657, 2004.
30. Lew ED, Oh J, Burrola PG, Lax I, Zagórska A, Través PG, Schlessinger J and Lemke G: Differential TAM receptor ligand phospholipid interactions delimit differential TAM bioactivities. *Elife* 3, 2014.
31. Rankin EB, Fuh KC, Castellini L, Viswanathan K, Finger EC, Diep AN, LaGory EL, Kariolis MS, Chan A, Lindgren D, *et al*: Direct regulation of GAS6/AXL signaling by HIF promotes renal metastasis through SRC and MET. *Proc Natl Acad Sci USA* 111: 13373-13378, 2014.
32. Li Y, Ye X, Tan C, Hongo JA, Zha J, Liu J, Kallop D, Ludlam MJ and Pei L: Axl as a potential therapeutic target in cancer: Role of Axl in tumor growth, metastasis and angiogenesis. *Oncogene* 28: 3442-3455, 2009.